Quantification of QLCS Tornadogenesis, Associated Characteristics, and Environments across a Large Sample

JAMES S. GOODNIGHT,[a] DEVIN A. CHEHAK,[b] AND ROBERT J. TRAPP[a]

[a] *Department of Atmospheric Sciences, University of Illinois at Urbana–Champaign, Urbana, Illinois*
[b] *National Weather Service, Midland, Texas*

(Manuscript received 28 January 2022, in final form 9 August 2022)

ABSTRACT: The skillful anticipation of tornadoes produced by quasi-linear convective systems (QLCSs) is a well-known forecasting challenge. This study was motivated by the possibility that warning accuracy of QLCS tornadoes depends on the processes leading to tornadogenesis, namely, one that is dominated by an apparent release of horizontal shearing instability [shearing instability dominant (SID)] and one by a pre-tornadic mesocyclone [pre-tornadic mesocyclone dominant (PMD)] and its associated generative mechanisms. The manual classification of the genesis of 530 QLCS tornadoes as either SID or PMD was performed using heuristic, yet process-driven criteria based on single-Doppler radar (WSR-88D) data. This included 214, 213, and 103 tornadoes that occurred during 2019, 2017, and 2016, respectively. As a function of tornadogenesis process, 36% were classified as SID, and 60% were classified as PMD; the remaining 4% could not be classified. Approximately 30% of the SID cases were operationally warned prior to tornadogenesis, compared to 44% of the PMD cases. PMD tornadoes were also more common during the warm season and displayed a diurnal, midafternoon peak in frequency. Finally, SID cases were more likely to be associated with QLCS tornado outbreaks but tended to be slightly shorter lived. A complementary effort to investigate environmental characteristics of QLCS tornadogenesis revealed differences between SID and PMD cases. MLCAPE was relatively larger for warm-season SID cases, and 0–3-km SRH was relatively larger in warm-season PMD cases. Additionally, pre-tornadic frontogenesis was more prominent for cool-season SID cases, suggestive of a more significant role of the larger-scale meteorological forcing in vertical vorticity that fosters tornadogenesis through SID processes.

KEYWORDS: Tornadoes; Radars/Radar observations; Mesoscale forecasting

1. Introduction

Quasi-linear convective systems (QLCSs) represent one of the main modes of organized convection that produce severe convective weather, primarily in the form of damaging surface winds and tornadoes (e.g., Smith et al. 2012). Across the United States, approximately 20% of all tornadoes are associated with QLCSs, with higher percentages in regions such as the Midwest and southeast (Trapp et al. 2005; Smith et al. 2012; Ashley et al. 2019). Relative to their supercell storm counterparts, QLCS tornadoes are known to present less warning lead time based on traditional Doppler radar indicators, with an average lead time between 5 and 10 min (Trapp et al. 1999; Brotzge et al. 2013). QLCS tornadoes also tend to occur relatively more frequently during the cool season and overnight hours than do supercell tornadoes (e.g., Trapp et al. 2005; Ashley et al. 2019); overnight tornadoes result in disproportionately more fatalities (Ashley et al. 2008). While QLCSs may not produce strong or violent tornadoes as often as supercells (Trapp et al. 2005; Smith et al. 2012; Brotzge et al. 2013), their tendency to occur overnight, during the cool season, and with comparatively little lead time can present a challenge to forecasters.

A review of the literature (e.g., Forbes and Wakimoto 1983; Funk et al. 1999; Trapp and Weisman 2003; Wheatley and Trapp 2008; Atkins and St. Laurent 2009; Schenkman et al. 2012; Conrad and Knupp 2019; Sherburn and Parker 2019; Flournoy and Coniglio 2019; Boyer and Dahl 2020; Marion and Trapp 2021) suggests that QLCS tornadogenesis can be characterized in two general ways, based on what appear to be the dominant processes. The first encompasses the sequence of processes involving mesocyclonic rotation thought to lead to tornadoes in most supercells (e.g., Davies-Jones et al. 2001), and accordingly, this is classified herein as pre-tornadic mesocyclone dominant (PMD). In generally reverse chronological order, such processes include the generation of: near-ground, mesocyclonic-scale rotation, most likely originating at least in part from storm-generated, horizontal baroclinic vorticity (e.g., as originally described by Rotunno and Klemp 1985 and Davies-Jones and Brooks 1993) cloud-base rotation and its dynamical lifting, which acts to stretch vertical vorticity of the near-surface parcels (e.g., Markowski and Richardson 2014); and a midlevel (e.g., 2–7 km AGL) mesocyclone, which helps in part to condition the storm for horizontal baroclinic vorticity generation (e.g., Brooks et al. 1994). Numerous modeling studies have displayed a PMD sequence occurring in QLCSs. For example, Trapp and Weisman (2003) used simulations to show that tilting of baroclinic vorticity by downdrafts produced anticyclonic and cyclonic near-surface vortex pairs within a simulated QLCS, which were then stretched by leading-edge updrafts. Tilting of environmental horizontal contributed to midlevel mesovortices, which developed prior to those at low levels. Other studies (e.g., Atkins and St. Laurent 2009; Schenkman et al. 2012; Sherburn and Parker 2019; Flournoy and Coniglio 2019; Boyer and Dahl 2020; Marion and Trapp 2021)

Corresponding author: Robert J. Trapp, jtrapp@illinois.edu

DOI: 10.1175/WAF-D-22-0016.1

provide additional model-based evidence for PMD behavior in QLCSs. Inherently, a case classified as PMD is expected to provide a longer warning lead time prior to tornadogenesis.

It is relevant to note here that some of the theoretical basis for the "three-ingredients method" (3IM) proposed by Schaumann and Przybylinski (2012) stems at least in part from modeling studies of warm-season QLCSs exhibiting PMD processes (Rotunno et al. 1988; Trapp and Weisman 2003; Atkins and St. Laurent 2009). In the 3IM, a balance between low-level shear and system cold-pool leading to upright updrafts, 0–3-km line-normal environmental bulk shear greater than 15 m s^{-1}, and outflow-induced bowing in the line, are the "ingredients" considered to be conducive to tornadogenesis within QLCSs. Case studies have shown that the 3IM works well for forecasting certain QLCS tornadoes, especially for warm-season events (Brusky et al. 2015; Bentley and Logsdon 2016; see also Gibbs 2021). Indeed, this method appears to be particularly relevant for identifying PMD events, as outflow associated with a descending rear-inflow jet (RIJ) is consistent with tilting of baroclinic vorticity into the vertical.

In QLCS cases such as described by Conrad and Knupp (2019), tornadogenesis appears to be dominated by the release of horizontal shearing instability (HSI), and thus are classified herein as shearing instability dominant (SID). HSI is a type of barotropic instability that, when released, converts a zone of horizontal shear and associated sheet of vertical vorticity into discrete, like-signed vortices. The resulting pattern of vorticity is strongest near the surface and drops off quickly with height, as shown in simulations (e.g., Lee and Wilhelmson 1997a,b) and radar observations (Mueller and Carbone 1987; Conrad and Knupp 2019). Buban and Ziegler (2016a) show that this transition from shear vorticity to discrete vortices occurs on a time scale of between 5 and 15 min, depending on the strength of the initial vorticity. This comparatively short time scale of vortex formation may result in poor warning lead time, should such vortex formation result in tornadogenesis. Buban and Ziegler (2016b) also show that the resulting vortices are separated by approximately 7.9 times the width of a baroclinic shear zone, in general agreement with linear theory (e.g., Miles and Howard 1964). The vortex-spacing, shear–zone–width relationship has been used in past studies to argue the existence of HSI in QLCSs (Conrad and Knupp 2019). Rayleigh and Fjørtoft criteria (Rayleigh 1879; Fjørtoft 1950), which quantify the kinematic conditions across a zone of horizontal shear necessary to support the existence of HSI, can also be evaluated given sufficient information about the wind fields, and thus used to provide further evidence for HSI tornadogenesis within QLCSs (Conrad and Knupp 2019).

HSI has been proposed as a tornadogenesis mechanism within meteorological boundaries such as frontal rainbands (Carbone 1982; Clark and Parker 2014), trough lines (Wilson 1986) and thunderstorm outflow (Mueller and Carbone 1987). The requisite vertical vortex sheet associated with these boundaries can originate through different processes. For relatively short-lived (~1 h) thunderstorm outflow, tilting by updrafts or downdrafts of environmental or storm-generated horizontal vorticity is the most likely explanation (e.g., Markowski et al. 2014). For synoptic-scale fronts, or zones of mesoscale convergence, including the leading edges of long-lived ($\gtrsim$3 h) QLCSs and associated cold pools, the stretching of planetary vorticity readily explains prefrontal strips of vertical vorticity $\gtrsim 10^{-3}$ s^{-1} (e.g., Bluestein 1993, p. 302; see also Trapp 2013, p. 224), although a contribution from tilting is also possible. Because these details are difficult to disentangle even with high-resolution, research-quality data or modeling, attribution of the vortex sheet to a specific process will not be attempted herein.

While Conrad and Knupp (2019) and some of the other studies discussed above directly associate tornadogenesis with the HSI-generated vortices, other research suggests that stretching of these vortices may be necessary to produce a tornadic vortex (Wilson 1986; Brady and Szoke 1989; Wakimoto and Wilson 1989). In contrast, Lee and Wilhelmson (1997a) showed that local maxima of convergence between adjacent vortices act as favored regions for new updraft development, which can then stretch vorticity within the shear zone. In either case, stretching appears to play an important role in the generation of SID tornadoes.

The utility of the 3IM for the prediction of QLCS tornadoes generated through SID processes is less clear. The satisfaction of one or more of the 3IM conditions may be the effect of ongoing tornadogenesis due to HSI, rather than a cause of it. For example, local surges in the gust front—a 3IM requirement—are coincident with the release of HSI. In absence of clear guidance from the 3IM, and of midlevel vortices that would otherwise provide potentially longer lead times, we surmise that the SID tornadoes are key contributors to the relatively poor tornado-warning statistics associated with QLCSs (Brotzge et al. 2013). Insight into this statement, and into QLCS tornado prediction in general, requires evaluation of QLCS tornadogenesis over a large dataset. A heuristic yet process-driven methodology based on the use of a single-Doppler radar technique is established herein to conduct such an evaluation.

Motivated by the potential dependencies of tornado warning lead time, overall warning performance, and potential situational awareness on the dominant processes contributing to QLCS tornadogenesis, the primary objective of this study is to generate robust information on such contributing processes for applications in forecast and warning operations. Accordingly, the philosophical approach underlying our simple classification scheme of PMD versus SID is to focus on processes observable using operational data streams, while disregarding the details, which arguably are beyond the capabilities of, or need for, an operational forecaster to assess.

The specific goals of this study are therefore to: (i) quantify the relative occurrence of QLCS tornadogenesis through PMD versus SID processes, (ii) identify differences in the geospatial and temporal occurrences, associated tornado intensity, tornado warning performance, and other characteristics as a function of PMD versus SID processes, and (iii) describe the environmental conditions under which PMD versus SID tornadoes are more likely to occur. It is hypothesized that a tornado resulting from SID will have a shorter warning lead time than one resulting from PMD. Additionally, it is hypothesized that SID events will be more prevalent in the cool season along frontal boundaries with strong initial vertical vorticity. Finally, PMD events are hypothesized to be associated with stronger environmental CAPE and shear and thus more likely to occur during the warm season. These hypotheses will be addressed through analyses of single-Doppler radar data and analysis of tornadic QLCS environments. A multiyear study of QLCS tornadogenesis of this type is novel to the authors' knowledge and will provide new and operationally relevant insight into the environmental characteristics, lead times, and radar presentations of QLCS tornadogenesis.

2. Methods

An analysis of QLCS tornadoes during 2016, 2017, and 2019 was performed. These years represent a range of tornado frequency, with 2019 being the most active tornado year. Candidate QLCS tornado events were first determined by comparing local storm reports within the Storm Prediction Center (SPC) archive (www.spc.noaa.gov/archive/) to archived WSR-88D composite radar reflectivity images (www2.mmm.ucar.edu/imagearchive/). All official tornado reports were considered candidate cases for this study. For each candidate event, WSR-88D Level-II data (https://www.ncdc.noaa.gov/nexradinv/map.jsp) were obtained and analyzed using Gibson Ridge radar-viewing software (GR2Analyst) to objectively evaluate whether the event met QLCS criteria and then if so, to classify the tornadogenesis mechanism of the event (see below). To ensure the availability of low-level Doppler velocity data, the tornado and associated storm report must have occurred within 100 km of the nearest radar site: at this distance, the commonly used 0.5° elevation scan contains beams that sample the storm at around 1700 m above radar level (ARL). Also, to mitigate the effects of data dependency on our statistical analysis, the tornado must not have originated from the same low-level parent vortex as an immediately prior tornado, as determined by Doppler velocity data. There were several other reasons for the exclusion of an event from our tornado dataset. These included erroneous or unavailable data during tornadogenesis, the lack of observable low-level rotation at the time and location of the tornado report, or the transformation of the QLCS into discrete cells before tornadogenesis.

The date, time, season, latitude, longitude, and EF rating of each confirmed and included event were recorded using the NOAA-compiled storm events database (www.ncdc.noaa.gov/stormevents), which was taken to be the official source of the tornado reports within our QLCS tornado dataset. Here, a tornado was defined as a "cool season" event if it occurred from October to March and a "warm season" event if it occurred from April to September. Note that tornadoes rated EF-Unknown were included in the dataset but were not used in the analysis of genesis mechanism versus EF rating. Warning lead time was recorded based on the difference between the time of NWS tornado warning issuance and the time of the tornado report. Tornadoes that were not warned prior to genesis were assigned zero lead time.

a. *Manual radar data analysis*

To qualify as a QLCS, radar reflectivity of 40 dBZ at the 0.5° elevation angle must have been present continuously over a length of at least 75 km in any single direction at the time of tornadogenesis. This is similar to prior studies that have classified convective mode using radar (e.g., Trapp et al. 2005). The long-axis length of the QLCS was recorded along with the height of the lowest beam at the time and location of tornadogenesis. Additionally, characteristics such as the presence and strength of any associated midlevel circulation, the strength of a low-level tornadic circulation, and the presence of adjacent circulations were also determined based on Doppler velocity data. Here, the strength of circulation was defined as the maximum differential velocity across the vortex (ΔV; i.e., the difference between the maximum outbound and minimum inbound velocity) at the level of interest. The strength of the low-level tornadic circulation was used as an additional proxy for tornado strength (e.g., Toth et al. 2013) and complemented the EF rating assigned by the NWS. To more readily identify circulations within QLCSs, storm relative velocities were analyzed. The storm motion described in an NWS warning message was used when available; it otherwise was estimated by tracking the tornadic vortex in Doppler radar scans.

Finally, classification of each tornado event as either PMD or SID was performed using a set of radar-based criteria, as described next. In cases that did not meet all the criteria, the event was classified as "Other" and thus was not included in subsequent analysis.

1) TORNADOGENESIS THROUGH A PRE-TORNADIC MESOCYCLONE DOMINANT (PMD) PROCESS

Classification of a QLCS tornado event as PMD simply required a midlevel circulation before tornadogenesis. The insufficiency of a midlevel mesocyclone for tornadogenesis (Trapp et al. 2005) is fully acknowledged here, but the following criteria were employed to recognize the range limitations of operational weather radar and thus its ability to routinely detect near-surface rotation.

To be considered a midlevel circulation, a ΔV of at least 10 m s^{-1} between inbound and outbound peaks must have been observed at a height above 2 km, within 3 km of the line-relative location of the subsequent tornadic vortex. This circulation must have been observed three radar volume scans, or approximately 15 min, prior to the NOAA storm report. This is consistent with studies that identified midlevel circulations in both QLCSs and supercells (Trapp et al. 1999; Smith et al. 2012). An example of a PMD event is shown in Fig. 1.

2) TORNADOGENESIS THROUGH A SHEARING INSTABILITY DOMINANT (SID) PROCESS

It was not feasible to use single-Doppler velocity data to calculate the Rayleigh and Fjørtoft criteria, and thus identify necessary conditions theoretically supportive of HSI, over many cases. Therefore, an alternative approach based on a set

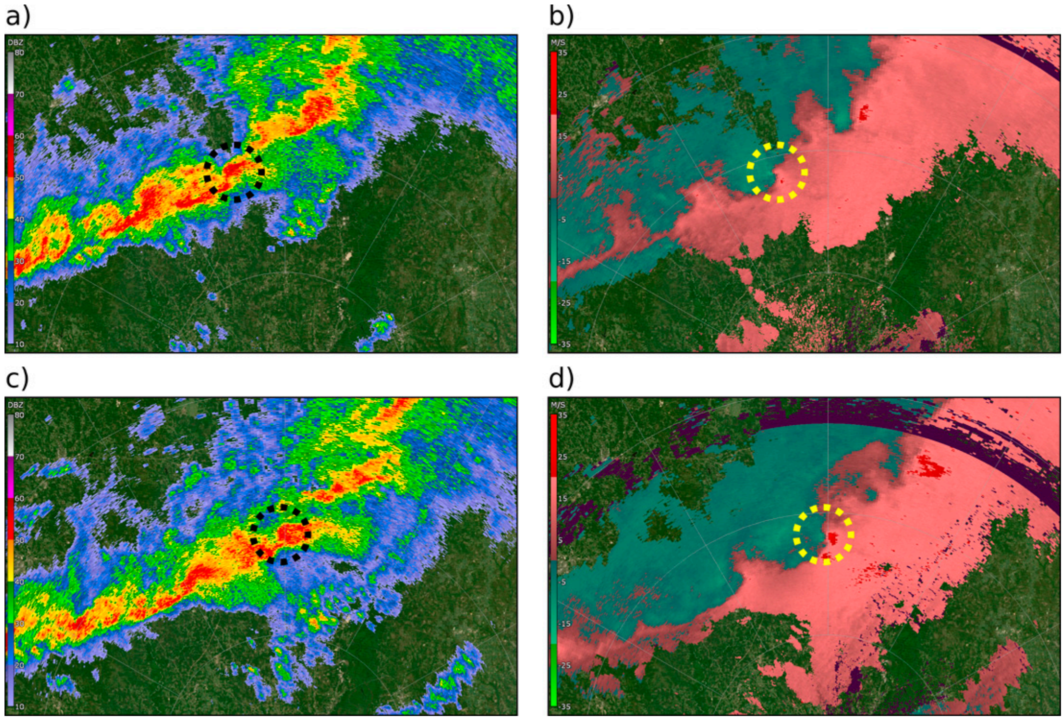

FIG. 1. Example of a QLCS exhibiting a tornadogenesis process dominated by a pre-tornadic mesocyclone, and thus classified as PMD, as represented in data from the Mobile, AL, WSR-88D (KMOB) on 3 Mar 2019. (a) The 1836 UTC radar reflectivity factor (hereafter, reflectivity; dBZ) at 0.5° elevation. (b) The 1836 UTC midlevel (>2 km) storm-relative radial velocity (m s^{-1}) at 1.3° elevation, 19 min before the tornado report. (c) The 1855 UTC reflectivity at 0.5° elevation. (d) The 1855 UTC storm-relative radial velocity at 0.5° elevation, at the time of tornadogenesis. The mid- and low-level circulations associated with the tornadic circulation are circled (~1000 m ARL).

of heuristically derived criteria was employed to identify HSI and thus quantify SID occurrence. Specifically, classification as SID required the presence of one or more low-level circulations adjacent to the tornadic vortex. This follows from the known breakdown of a shear zone into discrete vortices following the release of HSI, as revealed in modeling experiments (Lee and Wilhelmson 1997a; Buban and Ziegler 2016a,b) and in observations (e.g., Carbone 1982; Conrad and Knupp 2019). To be considered an adjacent circulation, it must have: formed within 25 km and three volume scans of the reported tornado, been associated with the parent QLCS, and had a maximum ΔV of at least 10 m s^{-1}, as viewed by the lowest elevation angle scan. It was not required that an adjacent circulation produce a tornado. Additionally, the existence of three or more adjacent low-level circulations that were evenly spaced (to within 1 km), including the tornadic circulation, was automatically considered to be an SID case regardless of the presence of a midlevel circulation.

To test its veracity in identifying an HSI process, these single-Doppler-based criteria were applied to the tornadic QLCS case analyzed by Conrad and Knupp (2019). They used 3D winds derived from dual-Doppler radar to confirm that the Rayleigh and Fjørtoft criteria were met, and that the necessary conditions for HSI were satisfied. The SID criteria described above were also satisfied for this case. This agreement with past results provides confidence in the single-Doppler methods used here. An example of a SID event is shown in Fig. 2.

To provide further support for our heuristically derived criteria, the shear zone width and distance between the resulting vortices following the (presumed) release of HSI were recorded in representative SID cases. This then allowed for a comparison with linear theory. Five SID cases in our database were identified to have been sampled such that radar beams were approximately parallel to the leading edge of the QLCS, prior to the release of HSI. The shear zone width was estimated by calculating the distance between maximum inbound and outbound velocity peaks across the leading edge of the QLCS. An example of this method is shown in Fig. 3.

Figure 3a shows the shear zone before the release of HSI, in the QLCS-relative location of subsequent release in Fig. 3b. In this case, a shear zone width of 1.0 km was estimated based on the distance between average inbound and outbound velocities (+12 and −17 m s^{-1}). In their idealized modeling studies, Buban and Ziegler (2016a,b) found that the most unstable wavelength resulting from the release of HSI is approximately 7.9 times the width of the shear zone both in barotropic and baroclinic flows. Using their results here, the most unstable wavelength would be 7.9×1.0 km $= 7.9$ km, which agrees well with the spacing observed between the

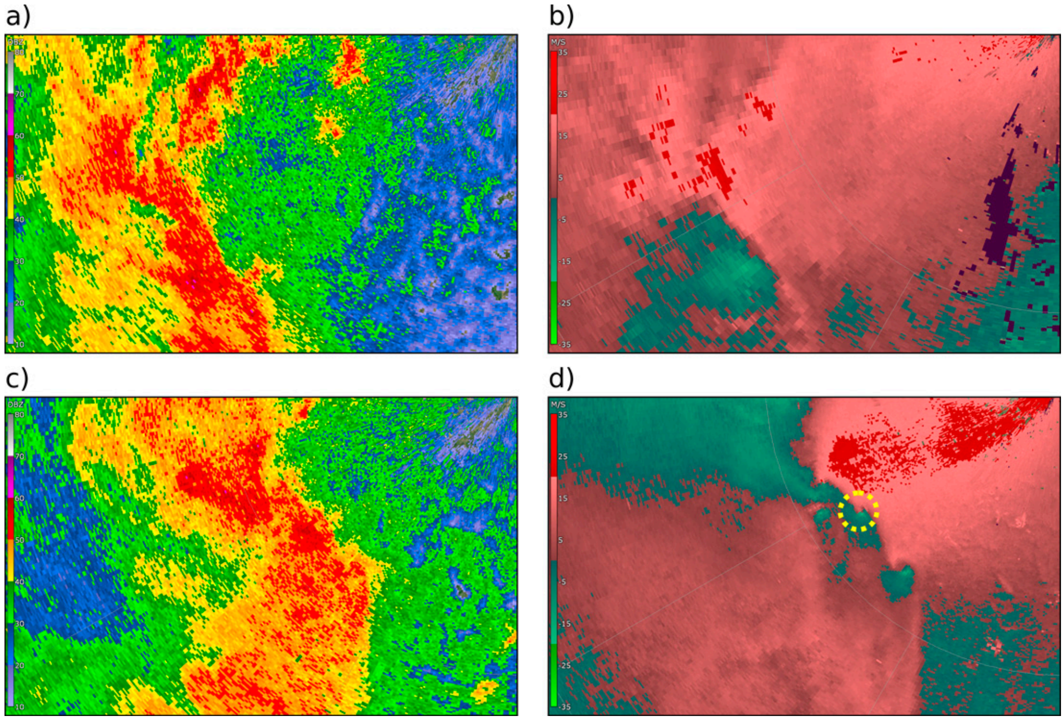

FIG. 2. Example of QLCS exhibiting a tornadogenesis process dominated by shearing instability, and thus classified as SID, as represented in data from the Austin/San Antonio, TX, WSR-88D (KEWX) on 20 Feb 2017. (a) The 0424 UTC reflectivity (dBZ) at 0.5° elevation. (b) The 0424 UTC midlevel (>2 km) storm-relative radial velocity (m s^{-1}) at 1.8° elevation. (c) The 0443 UTC reflectivity at 0.5° elevation. (d) The 0443 UTC storm-relative radial velocity at 0.5° elevation. The tornadic circulation is circled (~500 m ARL).

discrete vortices (Fig. 3b). Table 1 displays shear zone widths, observed wavelength, and wavelength predicted through linear theory for five SID cases in the database. This agreement with linear theory across multiple cases, in addition to the observation that the vortices are approximately evenly spaced, provides robust evidence that HSI was present and ongoing for these cases.

b. *Analysis of tornadic QLCS environments*

Pre-tornadic environments were investigated to determine their influence on tornadogenesis processes. Identification of environments that favor one process over the other would provide forecasters with increased situational awareness during QLCS events. For this study, the 13-km Rapid Refresh

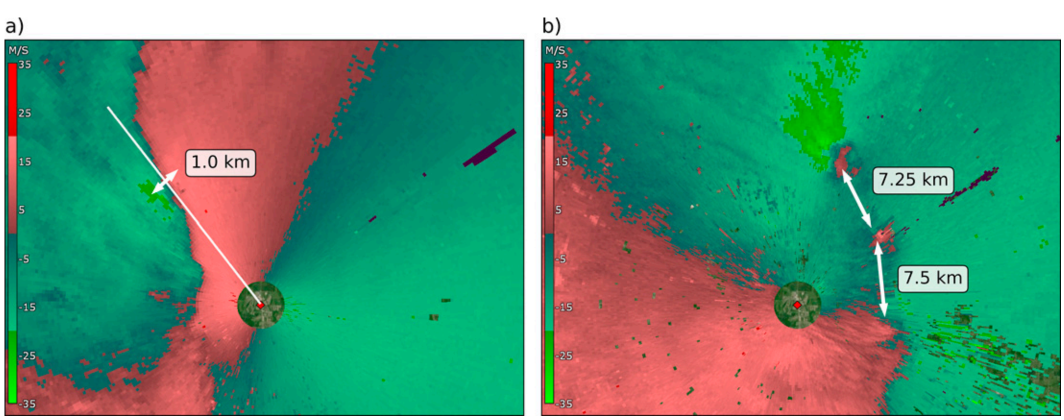

FIG. 3. Data from the Kansas City, MO, WSR-88D (KEAX) on 25 May 2019 displaying (a) 3.1° elevation storm-relative velocity (m s^{-1}; ~700 m ARL) used to estimate shear zone width and (b) 0.5° elevation storm-relative velocity (m s^{-1}) showing the subsequent release of HSI in the form of discrete vortices. The optimal radar viewing angle for this type of analysis is shown as a white line, and shear zone width and distances between vortices are shown with arrows.

TABLE 1. Observed shear zone width and resulting wavelength compared to that given by linear theory for five SID cases in the database.

Date	Observed shear zone width (km)	Observed wavelength of HSI (km)	Wavelength of HSI given by linear theory (km)
27 Apr 2016	2.0	14.5	15.8
7 Oct 2016	1.7	14.6	13.4
6 Mar 2017	1.7	12.3	13.4
25 May 2019	1.0	7.4	7.9
27 May 2019	1.5	13.5	11.9

(RAP) model analysis was chosen to evaluate pre-tornadic environments. Archived RAP data are available in 1-h increments throughout the years used in the QLCS tornado dataset. The latest RAP analysis available prior to the tornado storm report was chosen to represent the environment. For example, the 1600 UTC RAP analysis field was analyzed for a tornado occurring at 1630 UTC. Thus, there was a range of 0 and 59 min between the analysis time and the time of tornadogenesis.

Two subdomains of the RAP domain were used (Fig. 4). The first subdomain was 130 km × 130 km (11 × 11 grid points) in size and used to calculate all thermodynamic, kinematic, and composite parameters listed in Table 2. To allow for a range of possible QLCS orientations, QLCS motions, and associated inflow trajectories, this subdomain was centered meridionally and shifted one grid point zonally eastward relative to the tornado-report location (Fig. 4). The slight eastward shift was used to reduce the inclusion of postfrontal model soundings. Additionally, all thermodynamic and kinematic parameters within the subdomain were masked at model grid points where precipitation rate exceeded 0.001 kg m^{-2} s^{-1} or MUCAPE was less than 50 J kg^{-1} to eliminate the effects of parameterized convection and/or the effects of air that had been stabilized by a front or cold pool. The mean, median, and maximum parameter values were then calculated using non-masked grid points within the domain.

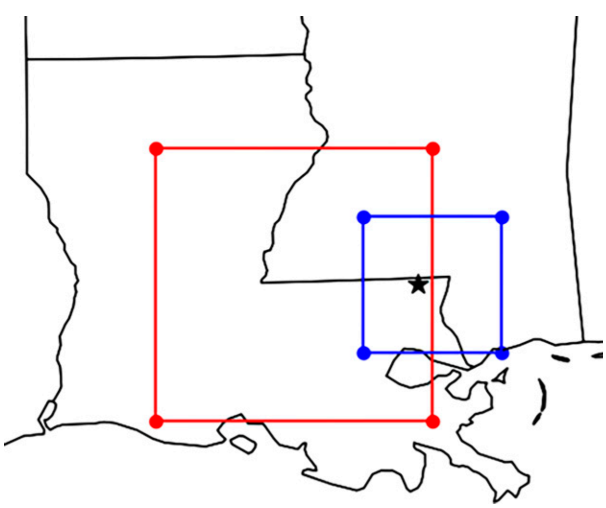

FIG. 4. Example of the two domains used for the environmental calculations. The location of the model grid point closest to the tornado storm report is marked with a star.

Parameter values at the model grid point closest to the tornado storm report were also recorded, as in Thompson et al. (2012). As noted in section 3, no major differences were found between these different representations of the environment.

The second subdomain was 260 km × 260 km (21 × 21 grid points) in size and was used to calculate parameters related to frontal forcing. This subdomain was centered meridionally and shifted 10 grid points (i.e., 130 km) westward relative to the tornado-report location (Fig. 4). The size and location of this subdomain were designed to sample the synoptic environment upstream of the location of tornadogenesis, assuming an average westerly storm motion.

To ensure independence of data, a tornado was excluded from the environmental analysis if its corresponding model-subdomain and time within the RAP analysis field were already sampled during another tornado case. In such instances, the stronger tornado was chosen to represent the environment at that time. There were seven such tornado cases removed, all of which formed via SID processes.

3. Results

a. *Occurrence and other characteristics as a function of dominant process*

530 QLCS tornado cases from 2016, 2017, and 2019 were identified and analyzed. The dominant process leading to QLCS tornadogenesis was determined to be SID in 190 cases (35.8%), PMD in 319 cases (60.2%), and "Other" in 21 cases (4.0%) (Table 3). Note that 21 "other" cases were neither preceded by a midlevel mesocyclone nor associated with adjacent circulations along the leading edge of the QLCS. The small number of these cases implies that either the SID or PMD classification account for a substantial proportion of QLCS tornadoes. Note also that the classification criteria allowed for each to occur in association with different tornadoes within the same QLCS. However, approximately 70% of all QLCSs exhibited a single dominant process (either PMD or SID) throughout their lifetime.

Following Trapp et al. (2005), confidence intervals for the percentage of QLCS tornadoes produced through either SID or PMD processes were estimated using statistical bootstrapping (Wilks 1995). Our dataset was resampled 10 000 times (with replacement). The bias-corrected and accelerated method of bootstrapping was then applied to the 10 000 synthetic datasets. The resultant 95% confidence intervals for the percentage of SID and PMD tornadogenesis, respectively, are

TABLE 2. Calculated environmental parameters. An asterisk indicates parameters that were calculated in the upstream subdomain.

Surface-based (SB) CAPE/CIN (J kg^{-1})	3–6-km lapse rate (°C km^{-1})	0–3-km storm-relative helicity (SRH) (Bunkers right storm motion) (m^2 s^{-2})
Most-unstable (MU) CAPE/CIN (J kg^{-1})	LCL height (m)	0–1-km bulk shear (m s^{-1})
0–3-km CAPE/CIN (J kg^{-1})	0–3-km layer-mean relative humidity (RH) (%)	0–3-km bulk shear (m s^{-1})
100-hPa mixed-layer (ML) CAPE/CIN (J kg^{-1})	3–6-km layer-mean relative humidity (RH) (%)	0–6-km bulk shear (m s^{-1})
RAP surface-based CAPE/CIN (J kg^{-1})	Significant tornado parameter (STP) (fixed layer)	Surface, 850-mb, and 700-mb frontogenesis (K m^{-1} s^{-1})*
0–1-km lapse rate (°C km^{-1})	Supercell composite parameter (SCP) (fixed layer)	Surface, 850-mb, and 700-mb vorticity (s^{-1})*
0–3-km lapse rate (°C km^{-1})	0–1-km storm-relative helicity (SRH) (Bunkers right storm motion) (m^2 s^{-2})	Surface, 850-mb, and 700-mb divergence (s^{-1})*

(31.7%, 39.8%) and (55.8%, 64.2%). Therefore, our estimates of SID and PMD tornadogenesis appear to be statistically significant at this level.

The possibility of a biased detection of PMD cases, which are more likely to be observed with increasing distance from radar (up to a certain range), was considered. Specifically, the dominant process for the subset of all cases that occurred within 50 km from the radar was examined. Of these 243 closer-range cases, 45% were found to be associated with SID, and 49% were found to be associated with PMD. Thus, even though this subset still has a relatively higher frequency of PMD cases, the possibility exists that the true percentage of tornadoes produced through SID may be even larger than shown here.

Figure 5 shows the geographical distribution of the QLCS tornado cases, separated based on season of occurrence and genesis process. Much of the cool season QLCS tornado activity occurred in the southeast United States, consistent with studies regarding the geographical location of high-shear, low-CAPE environments (Schneider et al. 2006; Sherburn and Parker 2014). Specifically, 75% of cool season cases occurred south of 37°N, an arbitrarily chosen latitude to distinguish northern and southern cases. On the other hand, 55% of warm-season cases occurred south of 37°N. In terms of genesis process, 61% of all SID cases occurred south of 37°N, while 66% of PMD cases occurred south of 37°N. Overall, there were 288 warm-season cases (54.3%) and 242 cool season cases (45.7%).

As detailed in Fig. 6a, a slightly higher proportion of SID cases occurred during the cool season relative to PMD cases; however, over half of all SID events occurred during the warm season. Both peak during the spring and follow a similar annual cycle (Fig. 6b). These results appear to disprove our hypothesis regarding a seasonal preference for SID and indicate the potential for PMD tornadogenesis during the cool season in the south, as well as SID tornadogenesis during the warm season in the north. We hypothesize that warm-season PMD tornadogenesis is more apt to occur in relatively long-lived QLCSs that have significant cold pools capable of concentrating planetary vorticity into a requisite vertical vortex sheet; evaluation of this hypothesis awaits the availability of proper datasets and/or innovative modeling experiments.

The time of tornadogenesis was converted to local standard time (LST) to evaluate the diurnal cycle of each dominant process. This is shown in Fig. 7. PMD cases have a clear diurnal peak of occurrence in the late afternoon, between the hours of 1500 and 1800 LST. Approximately 22% of all PMD tornadoes occurred during this period, compared to only 5% of SID tornadoes. This suggests that the contribution of solar heating is relatively more important for the development of PMD tornadoes than for SID tornadoes. In contrast, SID cases exhibit no clear diurnal peak, although there are periods of the day in which SID operates more frequently than PMD, particularly around 2000 LST (late evening) and around 1000 LST (early morning). Other studies have examined the diurnal distribution of tornadoes based on convective mode. Trapp et al. (2005) showed that tornadoes produced by discrete cells and QLCSs exhibit frequency peaks near 1800 LST, although for QLCS tornadoes this peak is less pronounced, with a larger fraction of QLCS tornadoes occurring overnight. By separating based on the dominant process leading to tornadogenesis, much of this observed mid- to late afternoon frequency peak in QLCS tornadoes can be attributed to PMD cases. Conversely, a greater fraction of overnight and morning tornadoes is produced through SID.

As noted in prior studies (e.g., Trapp et al. 2005) a disproportionate fraction of tornadoes produced by QLCSs are rated EF0 or EF1. Significant tornadoes (EF2+) are more likely to be produced by supercells. The distribution of tornadoes within our dataset is consistent with that of previous studies, as it includes only 39 significant tornadoes, none of which were EF4/5 (Fig. 8a). Additionally, more EF1 than EF0 tornadoes were recorded in this dataset (Fig. 8a), as was observed in separate analyses by Knupp (2000) and Trapp et al. (2005). This observation is likely due to the underreporting of weaker QLCS tornadoes, with damage done by EF0s

TABLE 3. Distribution of QLCS tornadoes as a function of dominant process and year.

Year	SID	PMD	Other	Total
2016	27	71	5	103
2017	89	117	7	213
2019	74	131	9	214
Total	190	319	21	530

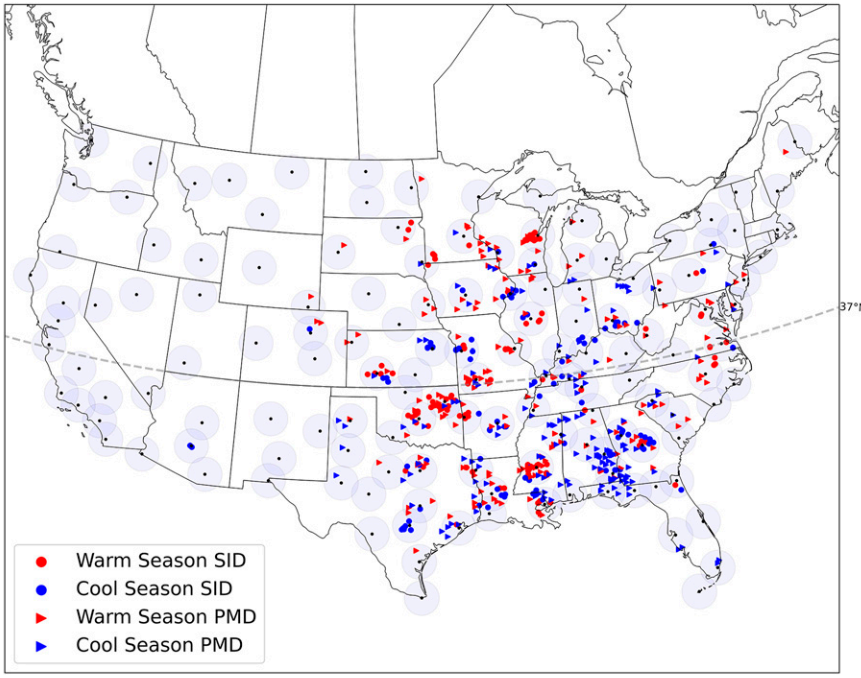

FIG. 5. Distribution of QLCS tornado cases by geographical location, season, and dominant process leading to tornadogenesis. The 100-km range rings for WSR-88Ds are shown as shaded circles. The 37°N parallel is also shown for reference.

remaining unreported or misrepresented as straight-line wind damage due to mesovortices (e.g., Trapp and Weisman 2003).

The radar-based strength of the tornadic circulation provides an alternative to EF rating because it is not susceptible to these reporting issues. The strength of the low-level circulation was defined as the maximum ΔV in the base scan immediately following tornadogenesis. The strength of the low-level tornadic circulation increases with the EF rating of the associated tornado (Fig. 8b), though substantial overlap exists (particularly between EF0 and EF1 tornadoes). This is consistent with Toth et al. (2013) who demonstrated that the strength of the tornadic circulation as measured by WSR-88D strongly correlates with "true" tornadic intensity as measured by mobile radar [the relationship between mobile radar measurements and EF rating is, however, not always straightforward (Snyder and Bluestein 2014)]. Subsequent research by Kingfield and LaDue (2015) also showed a correlation between peak ΔV and intensity estimates based on damage surveys. The conditional probability of a greater EF rating increases with peak ΔV (Smith et al. 2015, 2020), and along with STP can be used to estimate the EF rating of a given tornado in real time (Thompson et al. 2017). Each of these studies sampled tornadoes originating from supercells and

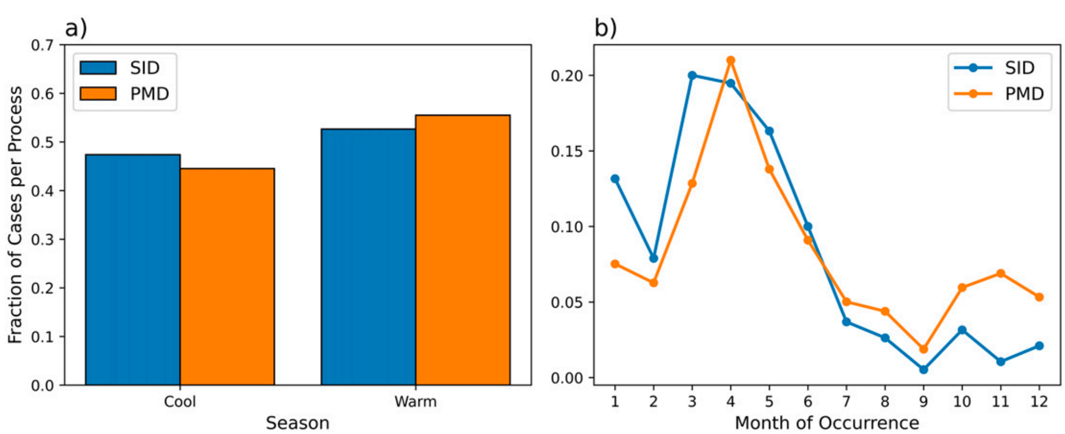

FIG. 6. QLCS tornadogenesis process as a function of (a) season of occurrence and (b) month of occurrence, normalized by the number of cases per process.

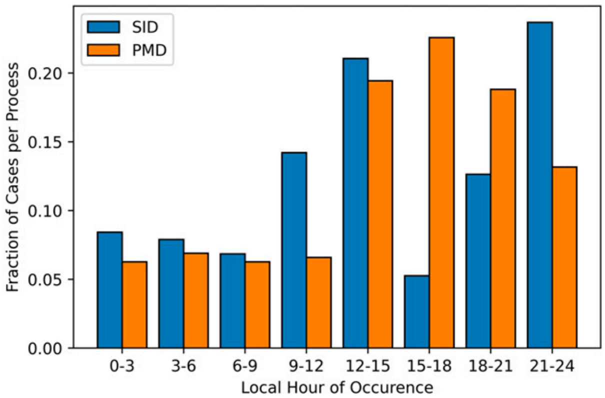

FIG. 7. QLCS tornadogenesis process as a function of local time of occurrence (LST), normalized by the number of cases per process.

QLCSs. The relationship between low-level tornadic vortex strength and EF rating in tornadic QLCSs specifically is further supported by results within this study.

Figure 9 shows the EF rating and low-level tornadic circulation strength for all cases separated based on the tornadogenesis process. For nonsignificant tornadoes (EF0–1), few differences exist between the distribution of SID and PMD based on EF rating. A slightly higher fraction (39.7%) of SID cases were associated with EF0 tornadoes compared to PMD cases (35.9%). The pattern of EF1 tornadoes being more common than EF0 tornadoes is consistent across both processes. 25 EF2 tornadoes were classified as PMD compared to 7 as SID. On average, the maximum ΔV sampled in the base scan was approximately 35 m s^{-1} for PMD cases, and 30 m s^{-1} for SID cases; for reference, the respective 10th and 90th percentile values of maximum ΔV were 23 and 48 m s^{-1} for PMD cases, and 21 and 40 m s^{-1} for SID cases. Due to the relatively unrestrictive definition of "low-level" by this study, the height at which this sampling occurred ranged between approximately 50 and 1500 m ARL, depending on the distance between the radar and tornadogenesis. If the data are constrained such that only storms sampled below 500 m are considered, the pattern of stronger PMD vortices remains. On average, a PMD process is more likely to lead to stronger tornadic vortices and significant tornadoes.

The depth and vertical structure of QLCS tornadic vortices also appear to depend on the tornadogenesis process. On average, SID tornadoes were sampled at a lower height than T&S tornadoes (Fig. 10a). In other words, using the stated criteria for determining dominant process, SID tornadoes were more readily observed when they occurred closer to a radar. There are likely two main reasons for this. SID tornadoes that occur farther from a radar may remain unreported and excluded from this database, especially if they are not associated with damage. Additionally, adjacent circulations (or even the tornadic vortices) may not be observed, leading to the tornado that would have otherwise been classified as SID being classified as "Other." This problem is not as evident for PMD tornadoes, given that a midlevel circulation is necessarily required to qualify a case as PMD.

To further address this, Fig. 10b shows the strength of the tornadic vortex by the dominant process, separated by EF-rating. Given two tornadoes with the same EF rating, one associated with a SID process and the other with a PMD process, it is more likely that the PMD tornado had a stronger circulation in the base scan. However, the damage at the surface was evaluated by the NWS to be produced by similar strength tornadoes. It is thus hypothesized that circulations associated with SID tornadoes decrease with height at a faster rate, i.e., are shallower than circulations associated with PMD. This has implications on situational awareness, as circulations associated with the apparent release of HSI may not necessarily be as strong at the height of the lowest radar beam relative to their ultimate EF rating, which could lead to the low probability of detection (POD) noted below for the SID tornadoes. Additionally, because of the lack of a midlevel circulation, the SID cases may have a stronger, downward-directed dynamic pressure gradient force (see

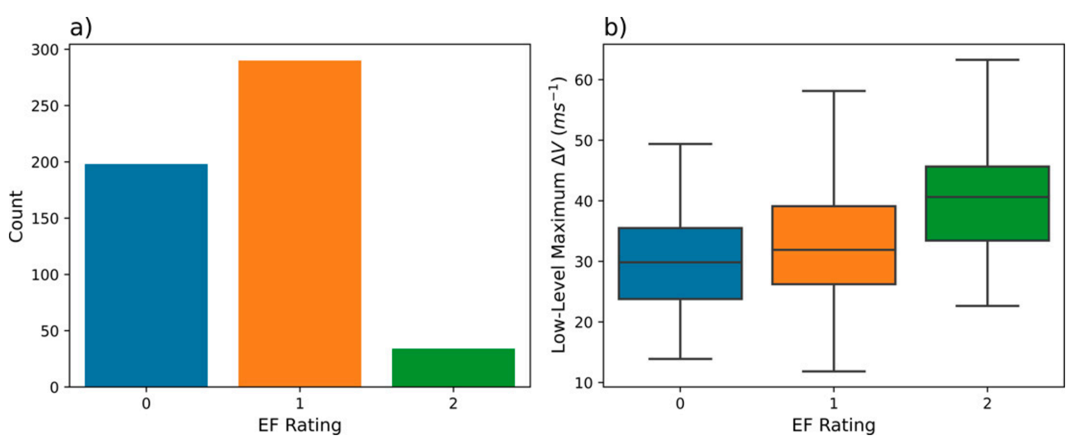

FIG. 8. (a) Total number of cases per EF rating category, as determined by NWS damage surveys, and (b) maximum ΔV (m s^{-1}) in the base scan immediately following the time of tornado occurrence, separated by EF rating. EF3 tornadoes are not included, as there were only two such instances in our dataset.

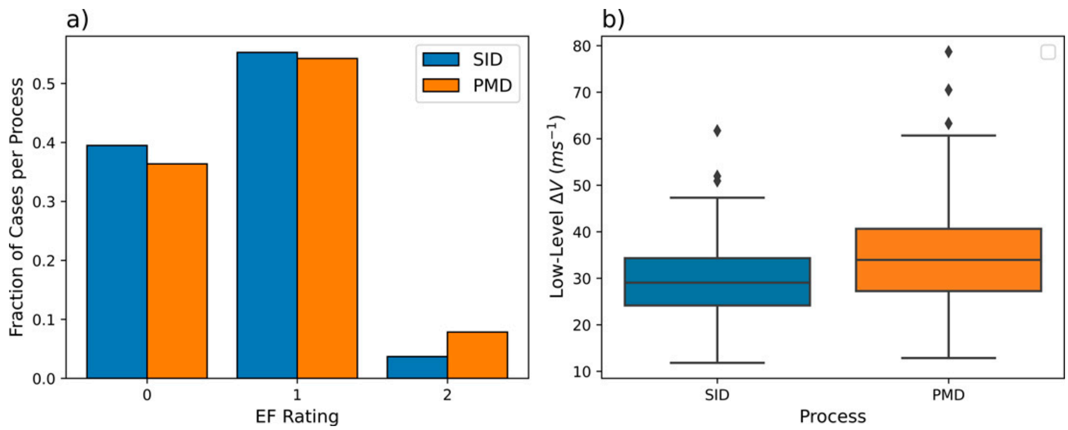

FIG. 9. (a) EF rating as a function of dominant process leading to tornadogenesis, normalized by total number of cases per process, and (b) maximum low-level ΔV (m s^{-1}) within the tornadic vortex as a function of tornadogenesis process.

Trapp 2013), which will inhibit updrafts and therefore limit tornado intensification and duration. Based on tornado duration recorded in the NCEI database, PMD tornadoes lasted approximately one minute longer than SID tornadoes on average (not shown).

SID cases were more likely to be associated with QLCS tornado outbreaks. Here, QLCS tornado outbreaks were defined as the occurrence of six or more QLCS tornadoes during one day (i.e., the period 1200–1200 UTC). In total, 22 out of 160 total "tornado days" within the database featured 6 or more tornadoes and accounted for 231 out of 530 total tornadoes. Of these tornadoes on outbreak days, 43% were SID. This is larger than the percentage of SID tornadoes in the entire database (36%), implying that the SID process played an enhanced role during QLCS outbreak days. We surmise that this is because PMD is more of a discrete process and associated with a single region of enhanced low-level vorticity. In contrast, the SID process is inherently associated with multiple vortices along the leading edge of a QLCS, each representing a potential zone of tornadogenesis.

Finally, it was suggested in section 1 that warning lead time could be inherently different for PMD versus SID tornadogenesis. 202 out of the 530 QLCS tornadoes in this dataset were warned by the NWS before tornadogenesis, yielding a POD of 0.381. The average NWS warning lead time across all cases, including those with zero lead time, was 4.8 min. For cases that were warned prior to tornadogenesis, SID and PMD cases had similar nonzero lead times of about 10 min. However, only 31.1% of SID cases were warned while 43.6% of PMD cases were warned. This discrepancy suggests a significant reduction in situational awareness during SID events, likely due to the absence of a midlevel circulation substantially prior to tornadogenesis. Current metrics and thresholds used within the NWS for issuance of warnings may not be well suited for the SID process leading to tornadogenesis.

b. *Near-storm environment as a function of dominant process leading to tornadogenesis*

Environmental parameters were evaluated using RAP analysis fields to explore possible differences between the environments

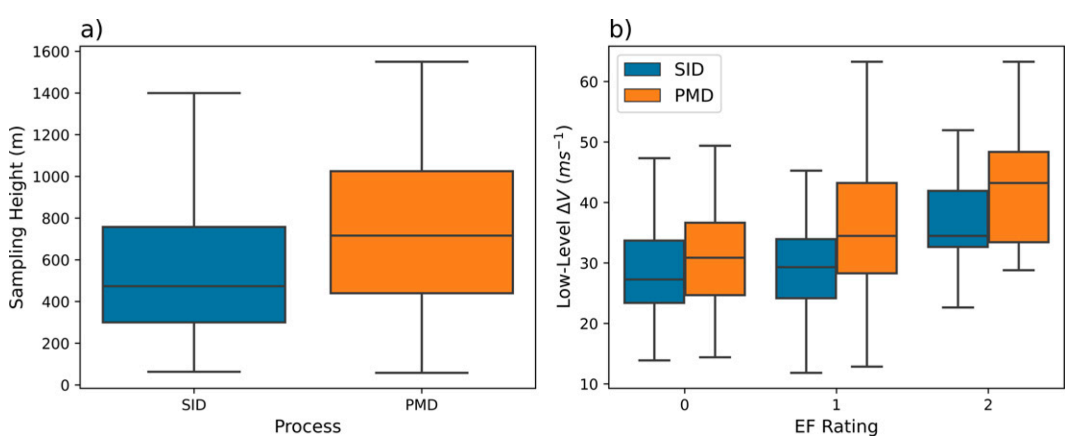

FIG. 10. (a) Height of the base scan at the time and location of tornado occurrence. (b) Maximum low-level ΔV (m s^{-1}) within the tornadic vortex as a function of EF rating, separated by tornadogenesis process.

TABLE 4. Mean domain-averaged parameter values separated by dominant process. The p values were determined using the Student's t test for differences between the mean values associated with each process. The letter "S" stands for surface.

	PMD	SID		PMD	SID		PMD	SID
SBCAPE (J kg^{-1})	896.0	966.5	0–1-km SRH (m^2 s^{-2})	269.0	248.8	STP	1.02	0.96
$p = 0.32$			$p = 0.08$			$p = 0.42$		
SBCIN (J kg^{-1})	85.9	98.9	0–3-km SRH (m^2 s^{-2})	368.9	329.7	0–3-km layer-mean RH (%)	80.5	77.9
$p = 0.13$			$p = 0.004$			$p = 0.002$		
0–3-km CAPE (J kg^{-1})	43.1	30.2	0–1-km bulk shear (m s^{-1})	16.2	16.5	3–6-km layer-mean RH (%)	65.5	55.7
$p = 0.002$			$p = 0.50$			$p < 0.001$		
0–3-km CIN (J kg^{-1})	30.6	30.2	0–3-km bulk shear (m s^{-1})	20.9	20.1	Domain max vorticity ($\times 10^{-4}$ s^{-1})	S: 2.09 (0.26) 850 mb: 3.20 (0.02)	S: 2.00 850 mb: 3.48
$p = 0.90$			$p = 0.09$				700 mb: 2.69 (0.02)	700 mb: 2.94
MUCAPE (J kg^{-1})	1242.3	1367.8	0–6-km bulk shear (m s^{-1})	27.6	26.7	Vorticity area	S: 35.3 (0.94) 850 mb:142.9 (0.53)	S: 35.1 850 mb: 138.5
$p = 0.11$			$p = 0.16$				700 mb: 93.8 (0.04)	700 mb: 105.8
MUCIN (J kg^{-1})	26.3	24.1	SCP	8.0	7.6	Domain max frontogenesis ($\times 10^{-8}$ C m^{-1} s^{-1})	S: 4.14 (0.02) 850 mb: 1.04 ($<$0.001)	S: 3.44 850 mb: 1.35
$p = 0.49$			$p = 0.41$				700 mb: 0.75 ($<$0.001)	700 mb: 1.01
MLCAPE (J kg^{-1})	843.6	1011.6	0–1-km lapse rate (C km^{-1})	5.5	5.5	Frontogenesis area	S: 57.9 (0.36) 850 mb: 64.0 ($<$0.001)	S: 55.3 850: 80.5
$p = 0.01$			$p = 0.63$				700: 33.5 ($<$0.001)	700: 50.2
MLCIN (J kg^{-1})	68.8	64.2	0–3-km lapse rate (C km^{-1})	5.7	5.5	Domain max convergence ($\times 10^{-4}$) (s^{-1})	S: 3.45 (0.37) 850: 2.21 (0.06)	S: 3.35 850: 2.34
$p = 0.40$			$p = 0.10$				700: 1.89 ($<$0.001)	700: 2.32
LCL height (m)	659.8	686.9	3–6-km lapse rate (C km^{-1})	3.3	3.5	Convergence area	S: 75.9 (0.184) 850 mb: 93.8 (0.61)	S: 79.5 850 mb: 96.2
$p = 0.31$			$p < 0.001$				700 mb: 55.4 ($<$0.001)	700 mb: 75.4

supporting SID versus PMD tornadogenesis. For each calculated parameter, the mean, median, and maximum value within the relevant analysis domain were recorded, as was the gridpoint value nearest to the location of tornadogenesis. No major differences were noted between these representations, and therefore the mean value was used in the analyses below. Table 4 lists the mean for all parameters, separated by the dominant process leading to tornadogenesis. Note that many parameters do not reveal significant differences between the dominant processes and thus were excluded from further analysis.

Surface-based (SB) and 100-hPa mixed-layer (ML) CAPE are shown in Fig. 11, separated both by season and process. It was hypothesized in section 1 that PMD cases would be associated with higher CAPE relative to SID cases, assuming the need in the PMD cases for relatively stronger updrafts to vertically tilt horizontal vorticity. However, SBCAPE associated with SID and PMD tornadoes shows little difference in distribution, even when separating across seasons. Using the mean values within the first (11 × 11) gridpoint analysis subdomain (Fig. 4), cool season QLCS tornado environments averaged about 570 J kg^{-1} of SBCAPE (SID = 563 J kg^{-1}, PMD = 569 J kg^{-1}), while warm season QLCS tornado environments averaged about 1200 J kg^{-1} of SBCAPE (SID = 1250 J kg^{-1}, PMD = 1150 J kg^{-1}). The difference in MLCAPE across the two mechanisms is more noticeable (and statistically significant; Table 4), especially during the warm season (Fig. 11b). The larger mean MLCAPE for warm-season SID would be consistent with our aforementioned idea about the possible higher likelihood of SID tornadogenesis within long-lived QLCSs, since QLCSs forming within higher CAPE environments are more likely to have stronger and deeper cold pools, and maintain updraft balance over a longer period (Weisman 1993; James et al. 2006). Overall, we conclude from this analysis that a wide range of CAPE values can support tornadogenesis through SID or PMD.

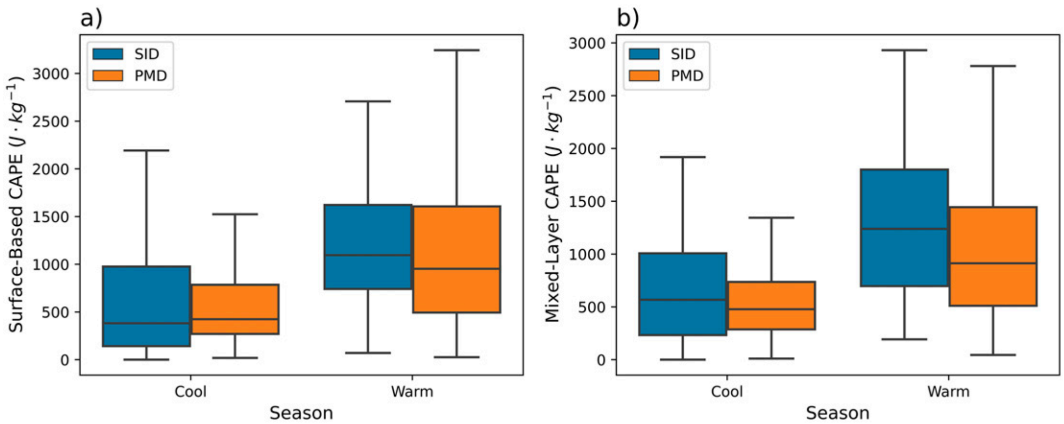

FIG. 11. Domain-averaged (a) surface-based and (b) mixed-layer CAPE as a function of dominant process, separated by season of occurrence.

Figure 12 shows environmental storm-relative helicity (SRH) and bulk shear over atmospheric layers typically used for severe storm forecasting. PMD events were expected to be associated with higher values of domain-mean 0–1- and 0–3-km SRH, given the existence of midlevel circulations produced through tilting of environmental vorticity. There is some evidence of this in Fig. 12b and Table 4, especially with 0–3-km SRH in the warm season. In general, SRH and bulk shear are greater in magnitude during the cool season, given the greater potential for synoptically driven frontal systems. Mean values of 0–6-km bulk shear are marginally stronger for SID events during the cool season, and consistently, there is some evidence that SID events are more strongly associated with an amplified upper-air pattern, based on higher values of upstream vorticity, frontogenesis, and convergence (Table 4). Mean 0–6-km bulk shear is also marginally stronger for PMD cases in the warm season. Overall, vertical wind shear appears to have more influence on convective mode than tornadogenesis mechanism in QLCSs.

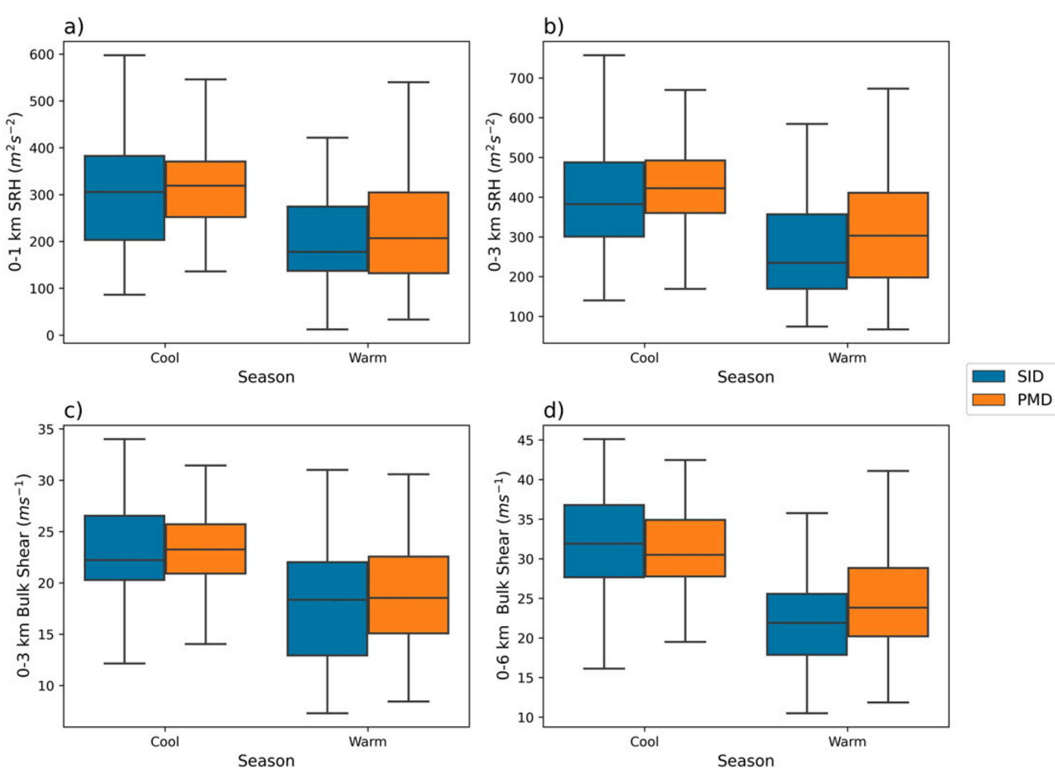

FIG. 12. Domain-averaged (a) 0–1-km SRH (m^2 s^{-2}), (b) 0–3-km SRH, (c) 0–3-km bulk shear (m s^{-1}), and (d) 0–6-km bulk shear as a function of dominant process leading to tornadogenesis, separated by season of occurrence.

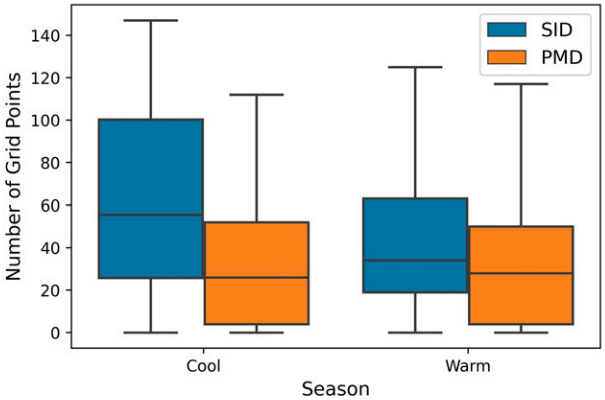

FIG. 13. Number of grid points (out of 200) where frontogenesis exceeds threshold value of 3×10^{-9} K m^{-1} s^{-1} at 700 hPa as a function of dominant process and season.

To test the hypothesis that SID events were relatively more likely to benefit from the forcing associated with fronts, 700-hPa frontogenesis was quantified by counting the number of grid points within the second (21×21 grid point) analysis subdomain (see Fig. 4) exceeding a threshold value, which was determined using scale analysis. This exceedance value at 700 hPa was 3×10^{-9} K m^{-1} s^{-1}.

The 700-hPa frontogenesis exceeds the threshold values over a larger area for SID cases than for PMD cases, especially during the cool season (Fig. 13). This is consistent with the hypothesis that QLCSs along frontal boundaries form within enhanced areas of vertical vorticity, increasing the chances that, over time, this vorticity will be concentrated within a sufficiently narrow pattern for the eventual release of HSI. It is noted that calculations of surface parameters such as vorticity and frontogenesis (see Table 4) reveal little difference between cool season SID and PMD cases, possibly due to contamination of these fields by the QLCS itself. Warm season QLCSs tend to not be associated with strong frontal forcing, as evidenced by low exceedance values across both mechanisms shown in Fig. 13. Thus, warm season SID and PMD cases show little difference in terms of frontogenesis.

4. Analysis of two representative cases

The following presents analyses of two QLCS cases that predominantly produced SID or PMD tornadoes. The PMD case occurred at 0105 UTC 17 June 2017 in eastern Nebraska, and the SID case occurred at 2049 UTC 29 December 2019 in central Mississippi. These cases were chosen because they fall within representative ranges of radar and environmental parameter values given in section 3.

a. Overview

The 17 June 2017 QLCS originated within a weak, nearly zonal 500-hPa pattern (Fig. 14a). Approximately 6000 J kg^{-1} of weakly capped, surface-based CAPE was present throughout southeastern Nebraska, with high 0–6-km shear of 25 m s^{-1}. Approximately 300 m^2 s^{-2} of 0–3-km SRH and 150 m^2 s^{-2} 0–1-km SRH was present. Initially discrete thunderstorms formed along surface convergence in central Nebraska before quickly organizing into a line, moving southeast in a direction nearly parallel to the 0–6-km shear vector. Tornadogenesis occurred approximately 3 h after convective initiation. In total, three separate tornadoes associated with the QLCS were included in our database, all classified as PMD.

The 29 December 2019 QLCS occurred downstream of a negatively tilted 500-mb (1 mb = 1 hPa) trough centered along the central U.S. Great Plains (Fig. 14c). An occluded surface cyclone was in southern Minnesota, with a cold front extending south across the Midwest and southern Great Plains (Fig. 14d). Throughout the day on 29 December, linear convection formed along the southern end of this front in the presence of weak CAPE and stronger forcing for ascent along the front. Deep-layer shear of 35 m s^{-1} was present beneath the poleward flow to the east of the trough. Surface-based CAPE increased to around 1000 J kg^{-1} as diurnal heating and southerly flow within the warm sector continued throughout the midafternoon. The formation of a mesolow near Louisiana along the pre-existing cold front led to the enhancement of low-level SRH. This environment initially supported tornadogenesis associated with SID processes, and then later, by PMD processes; the analysis below will focus solely on the initial tornadogenesis.

b. Radar evolution

At 0050 UTC 17 June 2017, 15 min before PMD tornadogenesis, a strong midlevel circulation was present within the QLCS. This circulation was sampled at around 2100 m ARL in the 6.5° elevation scan of the Omaha, Nebraska, WSR-88D (KOAX), with an analyzed maximum ΔV of 49 m s^{-1} (Fig. 15a). The midlevel circulation coincided with a local outflow surge (Fig. 15b). A low-level circulation that met the 10 m s^{-1} minimum ΔV requirement at the lowest elevation was first observed at 0053 UTC, 12 min prior to tornadogenesis (Fig. 15b). This low-level circulation was located directly beneath the broad midlevel circulation that had been present for approximately 15 min. Gradual strengthening of the low-level circulation occurred until it reached its maximum ΔV of 63 m s^{-1} at the time of tornadogenesis. The time of tornadogenesis is further supported by a reduction in correlation coefficient (not shown) collocated with the low-level parent vortex, indicative of debris associated with the tornado, or tornado debris signature (TDS). This TDS was present for 7 min until tornado dissipation at 0112 UTC. The presence of this midlevel circulation preceding the tornadic circulation and lack of adjacent circulations within 25 km along the convective line led to classification of the tornado as PMD.

At 2034 UTC 29 December 2019, or 15 min before SID tornadogenesis, there were no clear midlevel (or low-level; Fig. 16a) circulations present within the main convective line, which was sampled at around 2400 m by the Jackson, Mississippi, WSR-88D (KDGX) at the 1.8° elevation angle (not shown). Around 2042 UTC, 7 min prior to tornadogenesis, the low-level circulation (ΔV = 13 m s^{-1}) associated

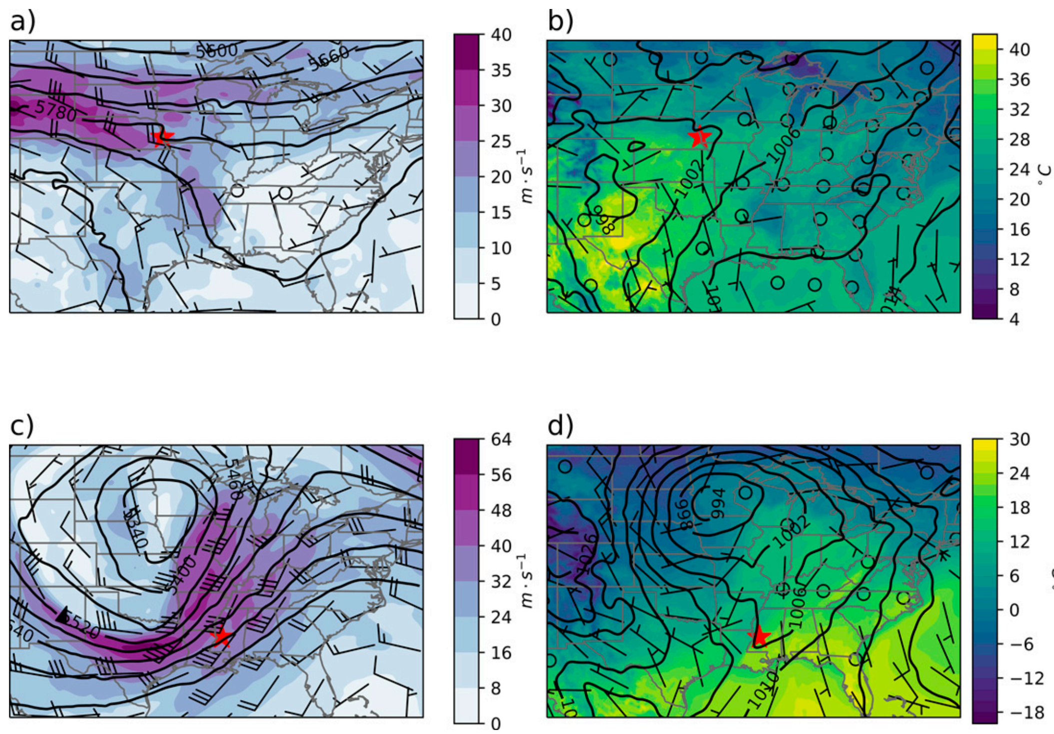

FIG. 14. RAP analysis 500-hPa geopotential height (m) and winds (m s^{-1}) at (a) 2000 UTC 29 Dec 2019 (SID case) and (c) 0100 UTC 17 Jun 2017 (PMD case). RAP analysis MSLP (hPa), surface winds (m s^{-1}), and temperature (°C) at (b) 2000 UTC 29 Dec 2019 and (d) 0100 UTC 17 Jun 2017.

with eventual tornadogenesis appeared on the 0.3° elevation scan, as did a midlevel circulation (ΔV = 14 m s^{-1}) on the 1.8° scan. Additionally, a circulation (ΔV = 17 m s^{-1}) approximately 9 km to the north, and another, weaker circulation (ΔV = 11 m s^{-1}) 9 km to the south appeared at this time on the 0.3° scan. The simultaneous appearance of these three, evenly spaced vortices with no preceding midlevel circulations seemingly signifies the release of HSI. This is apparent in the Doppler velocity field (Fig. 16b) as well as in the fields of radar reflectivity and spectrum width (Figs. 16c,d). The reflectivity field exhibits hook-like patterns as precipitation is wrapped within and by the emerging circulations, while the spectrum width field exhibits discrete elliptical regions representative of turbulent circulations amidst the surrounding updraft (Fig. 16d).

Over the next 7 min, all three circulations strengthened until tornadogenesis occurred within the middle of the three circulations at 2049 UTC (Fig. 16b). At this time, the tornadic parent vortex reached its maximum strength of 27 m s^{-1}. A reduction in correlation coefficient was observed for approximately 3 min. All three circulations moved northeastward with identical storm motion until their dissipation.

c. *Analysis of the three-ingredient method*

Next, we evaluate the 3IM for these two cases. As noted in section 1, the 3IM is widely used in operational settings to determine the likelihood of QLCS tornadogenesis. Since this method is intended to be a prognostic tool, the 3IM criteria will be evaluated prior to tornadogenesis in both cases.

Figure 17 shows the reflectivity and radial velocity about 15 min before PMD tornadogenesis within the 17 June 2017 QLCS. The position of the updraft-downdraft convergence zone (UDCZ), as inferred from the radial velocity field, relative to leading-edge updrafts, as inferred from the gradient in reflectivity field, is often used operationally to determine the ability of the QLCS to maintain vertically upright updrafts according to RKW-theory (Rotunno et al. 1988). At this time, the QLCS was largely "cold-pool dominant" within the southern portion of the line, because the UDCZ had advanced beyond the zone of high reflectivity gradient (Fig. 17). The northern portion of the QLCS was "shear dominant," because moderate-to-high reflectivity leads the UCDZ. Based on the 3IM, tornadogenesis is favored where the QLCS is balanced or slightly shear-dominated. Consistently, the tornado in this case formed within the balanced, central portion of the line.

The 3IM additionally requires the existence of an outflow surge, evident in Fig. 16 (and cross sections; not shown). The outflow surges within a descending RIJ could tilt horizontal baroclinic vorticity into the vertical, resulting in a low-level mesovortex, as suggested by Trapp and Weismann (2003). Tornadogenesis eventually occurred to the north of this surge in the 17 June 2017 case. Finally, the 3IM requires at least 15 m s^{-1} of line-normal, 0–3-km bulk shear. Near and downstream of the near-balanced portion of QLCS, shear is westerly at 23 m s^{-1}. Given the northwest–southeast orientation of the line, the magnitude of line normal shear was approximately 23 m s^{-1} × sin(60°) = 20 m s^{-1}, which satisfied the 3IM requirement.

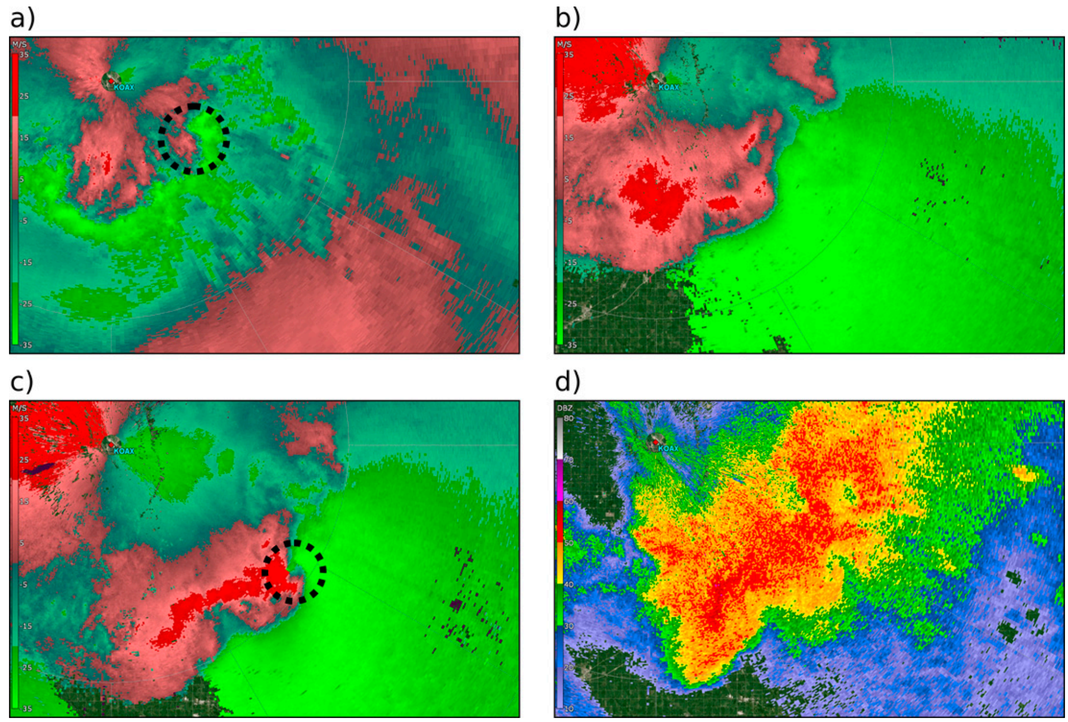

FIG. 15. Analysis of Omaha, NE, WSR-88D (KOAX) data on 17 Jun 2017: (a) 0050 UTC storm-relative radial velocity (m s^{-1}) at 6.5° elevation, (b) 0053 UTC storm-relative radial velocity at 0.5° elevation, (c) 0105 UTC storm-relative radial velocity at 0.5° elevation, and (d) 0105 UTC reflectivity at 0.5° elevation. Mid- and low-level circulations are circled (~350 m ARL).

Figure 18 shows the UDCZ and associated reflectivity field about 15 min prior to SID tornadogenesis in the 29 December 2019 QLCS. The QLCS was balanced/slightly shear dominant throughout its length, satisfying RKW balance criterion of the 3IM. Slight inflections within the velocity field could be interpreted as outflow surges. However, these inflections have much a lower amplitude in radial velocity than those in Fig. 17, more likely indicating that these inflections are the beginning of HSI release, clearly seen in Fig. 16. Thus, it is unclear whether the outflow surge criterion of the 3IM was satisfied. Finally, much of the 0–3-km bulk shear was line parallel. The difference between the line orientation angle and shear vector at the location of tornadogenesis is only about 15°, giving a line-normal shear magnitude of 25 m s^{-1} × sin(15°) = 6.5 m s^{-1}, lower than the 15 m s^{-1} requirement of the 3IM. Based on the 3IM for this sample case, it is unlikely tornadogenesis would be expected in the following 30 min. Our hypothesis is that a larger percentage of SID cases do not meet the 3IM criteria commonly used by NWS forecasters to predict QLCS tornadoes. While this claim is supported by lower POD of SID tornadoes, further analysis of the 3IM for more QLCS tornado cases is required.

5. Summary and conclusions

The primary objective of this project was to determine the climatological distribution of QLCS tornadoes as a function of the dominant process leading to tornadogenesis, specifically, shearing instability dominant (SID) and pre-tornadic mesocyclone dominant (PMD). This objective was motivated by hypothesized differences in the QLCS tornado warning accuracy and situational awareness offered by these two characterizations of tornadogenesis. Toward this end, the manual classification of 530 QLCS tornadoes as SID or PMD was performed using heuristic, yet process-driven criteria based on single-Doppler radar (WSR-88D) data. This included 214, 213, and 103 tornadoes that occurred during 2019, 2017, and 2016, respectively. As a function of dominant tornadogenesis process, 36% (190 tornadoes) were classified as SID, and 60% (319 tornadoes) as PMD; the remaining 4% could not be classified, based on our methodology.

Analysis of the climatological and radar characteristics of these tornado cases revealed important differences between QLCS tornadogenesis mechanisms. A late-afternoon, early-evening maximum (minimum) was indicated in the local time of PMD (SID) tornado occurrence. This implies a strong link of the PMD process to the diurnal heating cycle, and a dependence of the SID process on the larger-scale meteorological forcing. Relative to PMD tornadoes, a larger (smaller) fraction of SID tornadoes occurred during the cool (warm) season. However, this difference was not as significant as expected, as approximately 45% of SID tornadoes occurred during the warm season. It is possible that warm season tornadogenesis associated with HSI may be more likely in relatively long-lived QLCSs with significant cold pools capable of concentrating planetary vorticity into

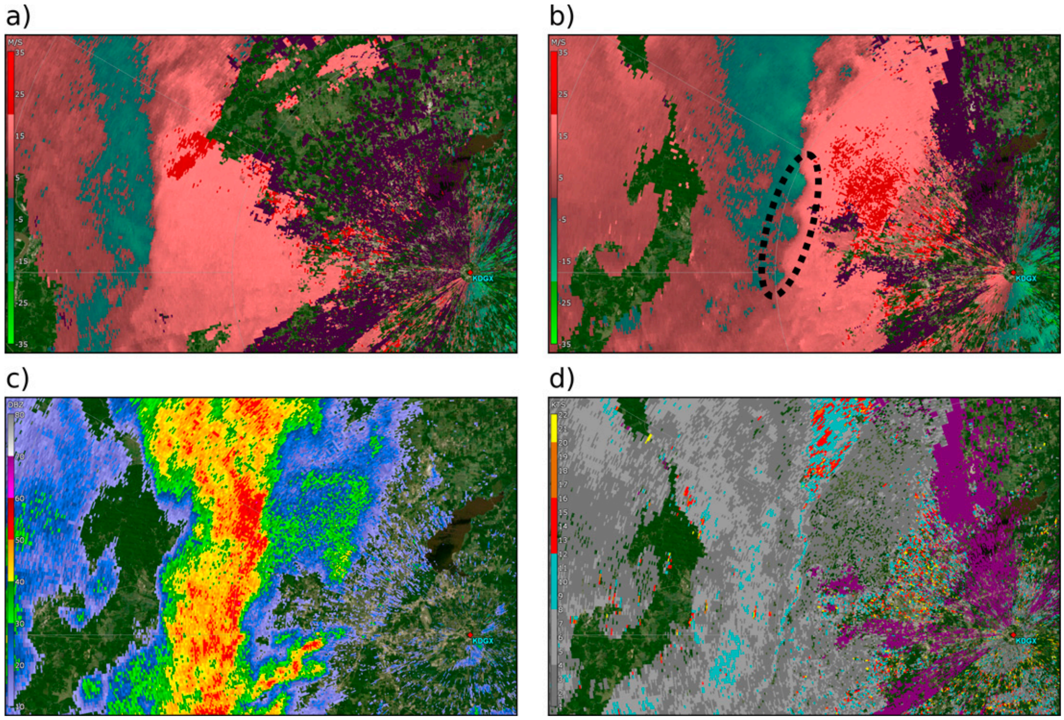

FIG. 16. Analysis of Jackson, MS, WSR-88D (KDGX) data on 29 Dec 2019: (a) 2038 UTC storm-relative radial velocity at 0.3° elevation, (b) 2054 UTC storm-relative radial velocity at 0.3° elevation, (c) 2054 UTC reflectivity at 0.3° elevation, and (d) 2054 UTC spectrum width at 0.3° elevation. Low-level circulations are circled (~450 m ARL).

a requisite vertical vortex sheet; this will be evaluated in future work.

Although there was little difference in the EF scale rating of SID versus PMD tornadoes, the radar-based quantification of the strength of the tornadic circulation showed that PMD genesis resulted in stronger tornadic circulations, as measured by maximum ΔV in our dataset. There was also little difference in the warning lead time as a function of the dominant process leading to tornadogenesis, as quantified for the subset of tornadoes that received NWS warnings prior to tornadogenesis. However, only 30% of SID tornadoes received warnings, as compared to 44% of PMD tornadoes. This could be due, in part, to the relative shallowness of the SID tornadoes compared to PMD tornadoes. This could also be due to the apparently greater weakening with height of tornadic vortices in SID cases relative to PMD cases, implying that the correlation between the strength of the tornadic vortex at the height of the radar beam and the strength of the tornado at the surface are inconsistent across mechanisms. This has implications on automated tornado detection methods and associated Doppler-velocity thresholds, as well as subjective criteria currently used operationally during the warning process. This also has implications on our finding that SID cases appear more

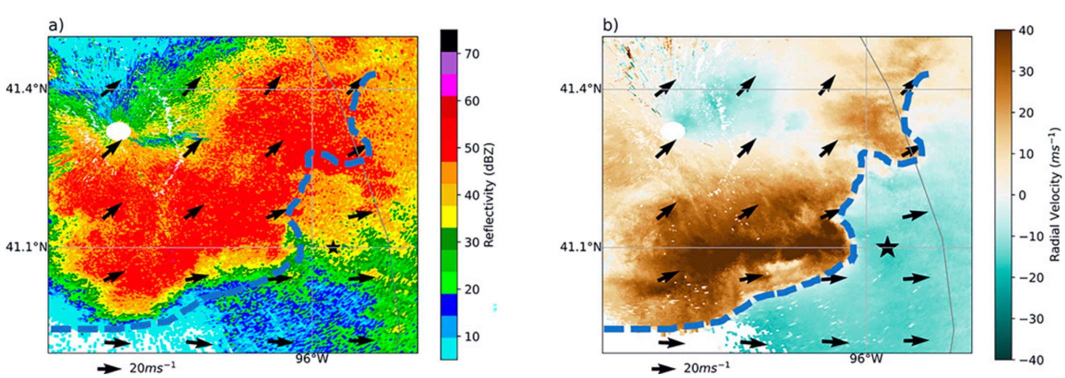

FIG. 17. Analysis of KOAX data on 17 Jun 2017: (a) 0055 UTC reflectivity (dBZ) at 0.5° elevation and (b) 0055 UTC radial velocity (m s^{-1}) at 0.5° elevation. The UDCZ is indicated by a bold dashed line. Vectors are of 0–3-km bulk shear (m s^{-1}) from the 0100 UTC RAP analysis field. The location of tornadogenesis at 0105 UTC is shown by the star.

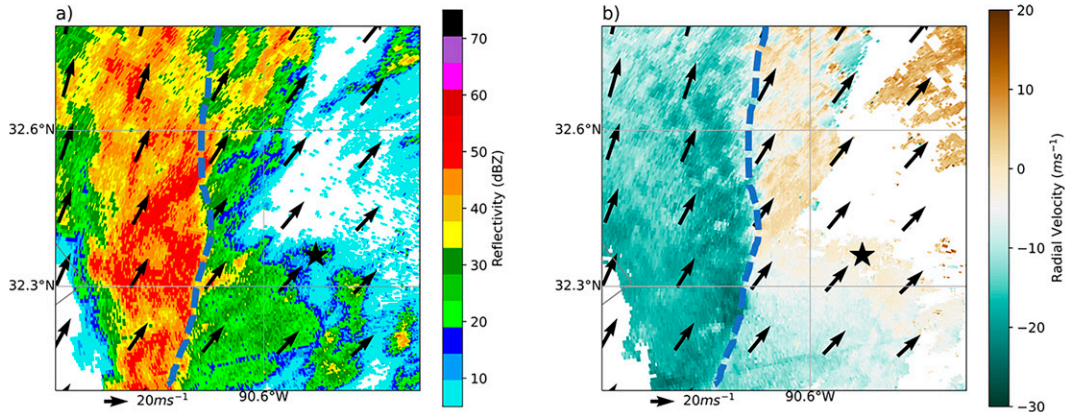

FIG. 18. As in Fig. 17, but for KDGX data on 29 Dec 2019: (a) 2031 UTC reflectivity (dBZ) at 0.5° elevation and (b) 2031 UTC radial velocity (m s^{-1}) at 0.5° elevation. Vectors are of 0–3-km bulk shear from the 2100 UTC RAP analysis field. The location of tornadogenesis at 2049 UTC is shown by the star.

likely to be associated with QLCS tornado outbreaks, but also tend to be slightly shorter lived.

A complementary effort to explore the environmental characteristics of QLCS tornadogenesis revealed a few distinct differences between SID and PMD tornadoes in terms of environmental parameters. In particular, we found evidence of relatively larger MLCAPE for warm-season SID cases, and relatively larger 0–3-km SRH in warm-season PMD cases. Additionally, pre-tornadic frontogenesis was more widespread and substantial for cool-season SID cases, suggestive of a more significant role of the larger-scale meteorological forcing in QLCS development as well as in the vertical vorticity that fosters the SID tornadogenesis.

Finally, case studies of two QLCSs representing PMD and SID tornadogenesis were conducted. Of most significance is that the SID case did not clearly exhibit the three primary criteria composing the three-ingredients method (3IM). Through a combination of additional data analyses and numerical modeling, future work will continue to explore the generalizability of the 3IM across different cases and seasons.

Acknowledgments. This work was supported by NOAA Award NA17OAR4590195. The authors are grateful for the comments and suggestions made by the three reviewers.

Data availability statement. Storm reports are available through NCEI (https://www.ncdc.noaa.gov/stormevents/). Level II radar data are available through NCEI (https://www.ncdc.noaa.gov/nexradinv/). RAP analysis fields are available through NCEI THREDDS server (https://www.ncei.noaa.gov/thredds/catalog/model-rap130-old/catalog.html). Environmental data were analyzed using MetPy (https://unidata.github.io/MetPy/latest/index.html).

REFERENCES

Ashley, W. S., A. J. Krmenec, and R. Schwantes, 2008: Vulnerability due to nocturnal tornadoes. *Wea. Forecasting*, **23**, 795–807, https://doi.org/10.1175/2008WAF2222132.1.

——, A. M. Haberlie, and J. Strohm, 2019: A climatology of quasi-linear convective systems and their hazards in the United States. *Wea. Forecasting*, **34**, 1605–1631, https://doi.org/10.1175/WAF-D-19-0014.1.

Atkins, N. T., and M. St. Laurent, 2009: Bow echo mesovortices. Part II: Their genesis. *Mon. Wea. Rev.*, **137**, 1514–1532, https://doi.org/10.1175/2008MWR2650.1.

Bentley, E. S., and J. R. Logsdon, 2016: An examination of the forecast process, mesoscale environment, and evolution of the northern Indiana/northwest Ohio derecho of 29 June 2012. *Electron. J. Severe Storms Meteor.*, **11** (1), https://ejssm.org/archives/2016/vol-11-1-2016/.

Bluestein, H. B., 1993: *Synoptic-Dynamic Meteorology in Midlatitudes. Volume II: Observations and Theory of Weather Systems*. Oxford University Press, 596 pp.

Boyer, C. H., and J. M. L. Dahl, 2020: The mechanisms responsible for large near-surface vertical vorticity within simulated supercells and quasi-linear storms. *Mon. Wea. Rev.*, **148**, 4281–4297, https://doi.org/10.1175/MWR-D-20-0082.1.

Brady, R. H., and E. J. Szoke, 1989: A case study of nonmesocyclone tornado development in northeast Colorado: Similarities to waterspout formation. *Mon. Wea. Rev.*, **117**, 843–856, https://doi.org/10.1175/1520-0493(1989)117<0843:ACSONT>2.0.CO;2.

Brooks, H. E., C. A. Doswell III, and J. Cooper, 1994: On the environments of tornadic and nontornadic mesocyclones. *Wea. Forecasting*, **9**, 606–618, https://doi.org/10.1175/1520-0434(1994)009<0606:OTEOTA>2.0.CO;2.

Brotzge, J. A., S. E. Nelson, R. L. Thompson, and B. T. Smith, 2013: Tornado probability of detection and lead time as a function of convective mode and environmental parameters. *Wea. Forecasting*, **28**, 1261–1276, https://doi.org/10.1175/WAF-D-12-00119.1.

Brusky, E., Jr., A. Allen, R. W. Przybylinski, and E. Townsend Jr., 2015: The tornadic quasi-linear convective system over east-central Wisconsin on 6–7 August 2013. Part 2: Radar and mesovortex analysis. *27th Conf. on Severe Local Storms*, Madison, WI, Amer. Meteor. Soc., 15B.6, https://ams.confex.com/ams/27SLS/webprogram/Paper254548.html.

Buban, M. S., and C. L. Ziegler, 2016a: The formation of small-scale atmospheric vortices via horizontal shearing instability.

J. Atmos. Sci., **73**, 2061–2084, https://doi.org/10.1175/JAS-D-14-0355.1.

——, and ——, 2016b: The formation of small-scale atmospheric vortices via baroclinic horizontal shearing instability. *J. Atmos. Sci.*, **73**, 2085–2104, https://doi.org/10.1175/JAS-D-14-0385.1.

Carbone, R. E., 1982: A severe frontal rainband. Part I: Stormwide hydrodynamic structure. *J. Atmos. Sci.*, **39**, 258–279, https://doi.org/10.1175/1520-0469(1982)039<0258:ASFRPI>2.0.CO;2.

Clark, M. R., and D. J. Parker, 2014: On the mesoscale structure of surface wind and pressure fields near tornadic and nontornadic cold fronts. *Mon. Wea. Rev.*, **142**, 3560–3585, https://doi.org/10.1175/MWR-D-13-00395.1.

Conrad, D. M., and K. R. Knupp, 2019: Doppler radar observations of horizontal shearing instability in quasi-linear convective systems. *Mon. Wea. Rev.*, **147**, 1297–1318, https://doi.org/10.1175/MWR-D-18-0257.1.

Davies-Jones, R., and H. E. Brooks, 1993: Mesocyclogenesis from a theoretical perspective. *The Tornado: Its Structure, Dynamics, Prediction, and Hazards, Geophys. Monogr.*, Vol. 79, Amer. Geophys. Union, 105–114.

——, R. J. Trapp, and H. B. Bluestein, 2001: Tornadoes and tornadic storms. *Severe Convective Storms*, C. A. Doswell III, Ed., Amer. Meteor. Soc., 167–221.

Fjørtoft, R., 1950: Application of integral theorems in deriving criteria of stability for laminar flows and for the baroclinic circular vortex. *Geophys. Publ.*, **17**, 1–52.

Flournoy, M. D., and M. C. Coniglio, 2019: Origins of vorticity in a simulated tornadic mesovortex observed during PECAN on 6 July 2015. *Mon. Wea. Rev.*, **147**, 107–134, https://doi.org/10.1175/MWR-D-18-0221.1.

Forbes, G. S., and R. M. Wakimoto, 1983: A concentrated outbreak of tornadoes, downbursts and microbursts, and implications regarding vortex classification. *Mon. Wea. Rev.*, **111**, 220–236, https://doi.org/10.1175/1520-0493(1983)111<0220:ACOOTD>2.0.CO;2.

Funk, T. W., K. E. Darmofal, J. D. Kirkpatrick, V. L. DeWald, R. W. Przybylinski, G. K. Schmocker, and Y.-J. Lin, 1999: Storm reflectivity and mesocyclone evolution associated with the 15 April 1994 squall line over Kentucky and southern Indiana. *Wea. Forecasting*, **14**, 976–993, https://doi.org/10.1175/1520-0434(1999)014<0976:SRAMEA>2.0.CO;2.

Gibbs, J. G., 2021: Evaluating precursor signals for QLCS tornado and higher impact straight-line wind events. *J. Oper. Meteor.*, **9**, 62–75, https://doi.org/10.15191/nwajom.2021.0905.

James, R. P., P. M. Markowski, and J. M. Fritsch, 2006: Bow echo sensitivity to ambient moisture and cold pool strength. *Mon. Wea. Rev.*, **134**, 950–964, https://doi.org/10.1175/MWR3109.1.

Kingfield, D. M., and J. G. LaDue, 2015: The relationship between automated low-level velocity calculations from the WSR-88D and maximum tornado intensity determined from damage surveys. *Wea. Forecasting*, **30**, 1125–1139, https://doi.org/10.1175/WAF-D-14-00096.1.

Knupp, K. R., 2000: Narrow streaks of "straight-line" wind damage. Do tornadoes or microbursts produce them? Preprints, *20th Conf. on Severe Local Storms*, Orlando, FL, Amer. Meteor. Soc., 644–645.

Lee, B. D., and R. B. Wilhelmson, 1997a: The numerical simulation of non-supercell tornadogenesis. Part I: Initiation and evolution of pretornadic misocyclone circulations along a dry outflow boundary. *J. Atmos. Sci.*, **54**, 32–60, https://doi.org/10.1175/1520-0469(1997)054<0032:TNSONS>2.0.CO;2.

——, and ——, 1997b: The numerical simulation of nonsupercell tornadogenesis. Part II: Evolution of a family of tornadoes along a weak outflow boundary. *J. Atmos. Sci.*, **54**, 2387–2415, https://doi.org/10.1175/1520-0469(1997)054<2387:TNSONT>2.0.CO;2.

Marion, G. R., and R. J. Trapp, 2021: Controls of quasi-linear convective system tornado intensity. *J. Atmos. Sci.*, **78**, 1189–1205, https://doi.org/10.1175/JAS-D-20-0164.1.

Markowski, P. M., and Y. P. Richardson, 2014: The influence of environmental low-level shear and cold pools on tornadogenesis: Insights from idealized simulations. *J. Atmos. Sci.*, **71**, 243–275, https://doi.org/10.1175/JAS-D-13-0159.1.

——, ——, and G. Bryan, 2014: The origins of vortex sheets in a simulated supercell thunderstorm. *Mon. Wea. Rev.*, **142**, 3944–3954, https://doi.org/10.1175/MWR-D-14-00162.1.

Miles, J. W., and L. N. Howard, 1964: Note on a heterogeneous shear flow. *J. Fluid Mech.*, **20**, 331–336, https://doi.org/10.1017/S0022112064001252.

Mueller, C. K., and R. E. Carbone, 1987: Dynamics of a thunderstorm outflow. *J. Atmos. Sci.*, **44**, 1879–1898, https://doi.org/10.1175/1520-0469(1987)044<1879:DOATO>2.0.CO;2.

Rayleigh, L., 1879: On the stability, or instability, of certain fluid motions. *Proc. London Math. Soc.*, **s1-11**, 57–72, https://doi.org/10.1112/plms/s1-11.1.57.

Rotunno, R., and J. Klemp, 1985: On the rotation and propagation of simulated supercell thunderstorms. *J. Atmos. Sci.*, **42**, 271–292, https://doi.org/10.1175/1520-0469(1985)042<0271:OTRAPO>2.0.CO;2.

——, ——, and M. L. Weisman, 1988: A theory for strong, long-lived squall lines. *J. Atmos. Sci.*, **45**, 463–485, https://doi.org/10.1175/1520-0469(1988)045<0463:ATFSLL>2.0.CO;2.

Schaumannn, J. S., and R. W. Przybylinski, 2012: Operational application of 0–3 km bulk shear vectors in assessing quasi linear convective system mesovortex and tornado potential. *26th Conf. on Severe Local Storms*, Nashville, TN, Amer. Meteor. Soc., 142, https://ams.confex.com/ams/26SLS/webprogram/Paper212008.html.

Schenkman, A. D., M. Xue, and A. Shapiro, 2012: Tornadogenesis in a simulated mesovortex within a mesoscale convective system. *J. Atmos. Sci.*, **69**, 3372–3390, https://doi.org/10.1175/JAS-D-12-038.1.

Schneider, R. S., A. R. Dean S. J. Weiss and P. D. Bothwell, 2006: Analysis of estimated environments for 2004 and 2005 severe convective storm reports. *23rd Conf. on Severe Local Storms*, St. Louis, MO, Amer. Meteor. Soc., 3.5, https://ams.confex.com/ams/23SLS/techprogram/paper_115246.htm.

Sherburn, K. D., and M. D. Parker, 2014: Climatology and ingredients of significant severe convection in high-shear, low-CAPE environments. *Wea. Forecasting*, **29**, 854–877, https://doi.org/10.1175/WAF-D-13-00041.1.

——, and ——, 2019: The development of severe vortices within simulated high-shear, low-CAPE convection. *Mon. Wea. Rev.*, **147**, 2189–2216, https://doi.org/10.1175/MWR-D-18-0246.1.

Smith, B. T., R. L. Thompson, J. S. Grams, C. Broyles, and H. E. Brooks, 2012: Convective modes for significant severe thunderstorms in the contiguous United States. Part I: Storm classification and climatology. *Wea. Forecasting*, **27**, 1114–1135, https://doi.org/10.1175/WAF-D-11-00115.1.

——, ——, A. R. Dean, and P. T. Marsh, 2015: Diagnosing the conditional probability of tornado damage rating using environmental and radar attributes. *Wea. Forecasting*, **30**, 914–932, https://doi.org/10.1175/WAF-D-14-00122.1.

——, ——, D. A. Speheger, A. R. Dean, C. D. Karstens, and A. K. Anderson-Frey, 2020: WSR-88D tornado intensity estimates. Part I: Real-time probabilities of peak tornado wind speeds. *Wea. Forecasting*, **35**, 2479–2492, https://doi.org/10.1175/WAF-D-20-0010.1.

Snyder, J. C., and H. B. Bluestein, 2014: Some considerations for the use of high-resolution mobile radar data in tornado intensity determination. *Wea. Forecasting*, **29**, 799–827, https://doi.org/10.1175/WAF-D-14-00026.1.

Thompson, R. L., B. T. Smith, J. S. Grams, A. R. Dean, and C. Broyles, 2012: Convective modes for significant severe thunderstorms in the contiguous united states. Part II: Supercell and QLCS tornado environments. *Wea. Forecasting*, **27**, 1136–1154, https://doi.org/10.1175/WAF-D-11-00116.1.

——, and Coauthors, 2017: Tornado damage rating probabilities derived from WSR-88D data. *Wea. Forecasting*, **32**, 1509–1528, https://doi.org/10.1175/WAF-D-17-0004.1.

Toth, M., R. J. Trapp, J. Wurman, and K. A. Kosiba, 2013: Comparison of mobile-radar measurements of tornado intensity with corresponding WSR-88D measurements. *Wea. Forecasting*, **28**, 418–426, https://doi.org/10.1175/WAF-D-12-00019.1.

Trapp, R. J., 2013: *Mesoscale-Convective Processes in the Atmosphere.* Cambridge University Press, 346 pp.

——, and M. L. Weisman, 2003: Low-level mesovortices within squall lines and bow echoes. Part II: Their genesis and implications. *Mon. Wea. Rev.*, **131**, 2804–2823, https://doi.org/10.1175/1520-0493(2003)131<2804:LMWSLA>2.0.CO;2.

——, E. D. Mitchell, G. A. Tipton, D. W. Effertz, A. I. Watson, D. L. Andra, and M. A. Magsig, 1999: Descending and nondescending tornadic vortex signatures detected by WSR-88Ds. *Wea. Forecasting*, **14**, 625–639, https://doi.org/10.1175/1520-0434(1999)014<0625:DANTVS>2.0.CO;2.

——, S. A. Tessendorf, E. S. Godfrey, and H. E. Brooks, 2005: Tornadoes from squall lines and bow echoes. Part I: Climatological distribution. *Wea. Forecasting*, **20**, 23–34, https://doi.org/10.1175/WAF-835.1.

Wakimoto, R. M., and J. W. Wilson, 1989: Non-supercell tornadoes. *Mon. Wea. Rev.*, **117**, 1113–1140, https://doi.org/10.1175/1520-0493(1989)117<1113:NST>2.0.CO;2.

Weisman, M. L., 1993: The genesis of severe, long-lived bow echoes. *J. Atmos. Sci.*, **50**, 645–670, https://doi.org/10.1175/1520-0469(1993)050<0645:TGOSLL>2.0.CO;2.

Wheatley, D. M., and R. J. Trapp, 2008: The effect of mesoscale heterogeneity on the genesis and structure of mesovortices within quasi-linear convective systems. *Mon. Wea. Rev.*, **136**, 4220–4241, https://doi.org/10.1175/2008MWR2294.1.

Wilks, D. S., 1995: *Statistical Methods in the Atmospheric Sciences: An Introduction*. International Geophysics Series, Vol. 59, Elsevier, 467 pp.

Wilson, J. W., 1986: Tornadogenesis by nonprecipitation induced wind shear lines. *Mon. Wea. Rev.*, **114**, 270–284, https://doi.org/10.1175/1520-0493(1986)114<0270:TBNIWS>2.0.CO;2.